JOURNAL OF PROPULSION AND POWER
Vol. 21, No. 2, March–April 2005

Oxidizer Control and Optimal Design of Hybrid Rockets for Small Satellites

Lorenzo Casalino* and Dario Pastrone†
Politecnico di Torino, 10129 Torino, Italy

The parameters that affect the design of a hybrid rocket for small satellites are highlighted, and the benefit of the oxidizer flow rate control is analyzed. A single-port circular-section polyethylene grain is considered; the oxidizer is 85% hydrogen peroxide. The engine design is optimized to search for the minimum engine mass when the initial satellite mass and the required velocity increment are assigned. First, the simplest blowdown feed system is considered. The analysis shows that the optimal design depends on a lower limit for the regression rate and sometimes on a further constraint, which is related to the occurrence of thermal choking. The initial values of the mixture ratio, the thrust level and the initial port area to the throat area ratio seem to be the most important parameters for an optimal design. As far as the oxidizer flow rate control is concerned, several control strategies, namely, constant mixture ratio, repressurization, constant combustion chamber pressure, and constant propellant tank pressure, are compared to the simplest blowdown system. The constant mixture ratio control is the worst case, as the mass and volume are similar to the blowdown case, while a large thrust variation occurs. Repressurization reduces the thrust variation. Constant pressure controls (both combustion chamber and tank pressures) guarantee a quasi-constant thrust and reduce engine dimensions, with a limited mass penalty.

Nomenclature

A_b	=	burning surface area, m^2
A_p	=	port area, m^2
A_t	=	nozzle throat area, m^2
a	=	regression constant, m$^{(1-2n)}$ (kg/s)^n
C_F	=	thrust coefficient
c	=	effective exhaust velocity, m/s
c^*	=	characteristic velocity, m/s
D	=	propellant tank diameter, m
F	=	thrust, N
G	=	mass flux, kg/(s m^2)
J	=	throat area to initial port area ratio
K_F	=	fuel mass flow coefficient
$\boldsymbol{k}$	=	vector of adjoint constants
L	=	overall length, m
m	=	mass, kg
n	=	mass-flux exponent
p	=	pressure, bar
R	=	radius, m
r	=	regression rate, m/s
s	=	wall thickness
t	=	time, s
V	=	volume, m^3
W	=	pressurizing gas work, J
$\boldsymbol{x}$	=	vector of design parameters
Z	=	hydraulic resistance, 1/(kg m)
α	=	mixture ratio
β	=	areal density, kg/m^2
ΔF	=	thrust variation, N
Δp_v	=	valve pressure drop, bar
ΔV	=	velocity increment, m/s
δ	=	constant, bar
ε	=	nozzle area ratio
μ	=	mass flow rate, kg/s
ρ	=	density, kg/m^3
$\boldsymbol{\chi}$	=	vector of constraining equations

Subscripts

a	=	auxiliary gas
b	=	burning
c	=	combustion chamber at nozzle entrance
cr	=	critical
e	=	propulsion system
F	=	fuel
f	=	final value
g	=	pressurizing gas
i	=	initial value
max	=	maximum
min	=	minimum
n	=	nozzle
O	=	oxidizer
p	=	overall propellant (oxidizer + fuel)
r	=	release repressurization gas
t	=	oxidizer propellant tank
u	=	initial ullage
1	=	combustion chamber at head end

Received 20 November 2003; revision received 17 May 2004; accepted for publication 20 May 2004.

*Associate Professor, Dipartimento di Energetica, C.so Duca degli Abruzzi 24. Member AIAA.

†Associate Professor, Dipartimento di Energetica, C.so Duca degli Abruzzi 24. Senior Member AIAA.

Introduction

IT is well known that hybrid rocket engines (HREs) present some interesting features that make this kind of engine safer than solid rocket motors and simpler than liquid rocket engines. HREs have a larger density impulse than liquid-bipropellant rocket engines and a larger specific impulse than solid rocket motors and liquid-monopropellant rocket engines. Moreover, HREs have a relatively low-cost, smooth throttling capability over a wide range of thrust levels, and shutdown-restart capability. These characteristics make HREs competitive for several applications, from large-scale rocket boosters to in-orbit thrusters. Several authors[1–10] have carried out numerical and experimental investigations on HREs. A large number of papers explore the application of hybrid rocket boosters to launch vehicles,[1–6] and, to a lesser extent, to upper stages,[7] sounding rockets,[8] and propulsion systems for small satellites.[9,10] More recently, a single-stage sounding rocket was built and tested by Lockheed Martin,[11] and the use of an HRE to power the Scaled Composite's SpaceshipOne[12] is considered. It has also been shown

that some propellants (cryogenic hybrid, paraffin and polyethylene waxes) can exhibit high regression rates, solving one of the main problems that affect HREs.[13,14] In Europe, there is interest in the application of small-scale HREs as a low-cost propulsion option for small satellites as an alternative to the hydrazine thruster.[9]

As far as the strategy to obtain high specific impulse from a given propellant combination is concerned, HREs are more complex than solid and liquid rockets, as the mixture ratio and combustion chamber pressure cannot be controlled independently. The required mixture ratio in solid rocket motors is a priori assigned, while the chamber pressure is dictated by the grain and nozzle geometry. Liquid engines can be operated at the proper chamber pressure, while maintaining the optimal mixture-ratio value. In the HRE, the fuel flow, which comes from the grain, does not vary in proportion to the oxidizer flow. Both the port area and exposed grain surface change during engine operations, and the mixture ratio shifts, even though the oxidizer mass flow is constant. The mixture-ratio shifting becomes less severe if the ratio between the final and initial radius is reduced, that is, if the burned web thickness is diminished or the initial port radius is increased. On the other hand, for a given oxidizer mass flow, a small port area, that is, high mass flux, is preferable to obtain high volumetric efficiency. The particular combustion process of HREs greatly influences the design of the solid grain and the control of the liquid propellant during operations. Finally, as far as the choice of the propellant combination is concerned, at least three elements are relevant: the thermochemical properties of the combustion gases as a function of the mixture ratio, the density of the propellants, and the grain regression rate.

In the present paper HREs for small satellites are considered, focusing attention on the parameters that affect the design. Moreover, an in-orbit use is considered, and no thrust level constraint is posed as would be, for instance, during an ascent trajectory. In this way one-lever propellant control is available. First, the simplest blowdown feed system is analyzed. In this case oxidizer flow rate control is not employed. A simple parametrical optimization of the design variables is performed. The effects of the oxidizer flow rate control on the design and performance of the HRE are then highlighted. In a previous work,[15] the optimal oxidizer flow rate control was considered. In the present work, the possible presence of suboptimal solutions, which trade a negligible amount of performance for a simpler control law, is investigated. The selected control strategies are constant mixture ratio, repressurization, constant chamber pressure, and constant propellant tank pressure.

The results presented here are for a specific application and propellant combination. Because of the peculiarity of HRE is not so easy to generalize results or find similitude rules. The same method can however be used to analyze different applications and propellant combinations.

Ballistic Model

The extensively considered propellant combination polyethylene (PE) and 85% hydrogen peroxide (85%HP) was chosen here. A popular code[16] is used to compute the properties of the combustion gases and rocket performance as a function of the mixture ratio α. Fourth-degree curve fits of the characteristic velocity and the thrust coefficient are embedded in the code to compute the proper values as the mixture ratio changes during engine operations. These fits are shown in Fig. 1 for $p_c = 10$ bar, $\varepsilon = 100$, and frozen equilibrium expansion. The product of c^* and C_F, that is, the effective exhaust velocity c, is also shown. Maximum values of c^*, c, and C_F are indicated by full circles. The data shown in Fig. 1 are adopted throughout to evaluate c^*, c, and C_F as functions of the varying mixture ratio, even though the actual pressure in the combustion chamber can assume different values during engine operations. The error is always lower than 2% over the range of chamber pressure and mixture-ratio values considered in this paper. Combustion efficiency, nozzle discharge coefficient, and nozzle efficiency are assumed to be unitary. The conservative assumption of frozen equilibrium expansion is adopted to compensate for the low combustion efficiency of HREs. Finally, an optimum value of ε that depends on the required velocity increment, the nozzle material, and the adopted cooling method can

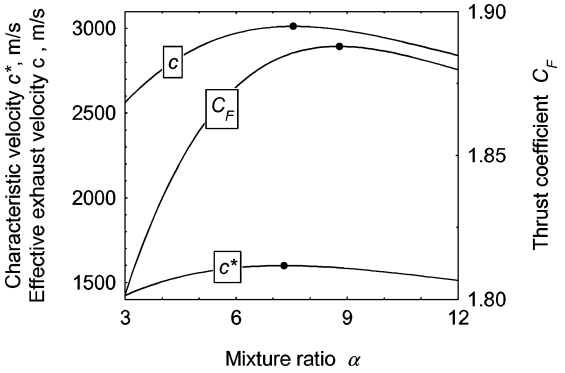

Fig. 1 Curve fits for characteristic velocity, effective exhaust velocity, and thrust coefficient for PE/85%HP as a function of the mixture ratio.

be found. For the sake of clarity, a fixed value $\varepsilon = 100$ is assumed unless otherwise specified. The effects of the nozzle area ratio have been analyzed separately, and some results are presented. The nozzle throat erosion is neither taken into account nor investigated. Nozzle inserts can be used to mitigate the erosion.

As far as the regression rate is concerned, the classical relation

$$r = aG_O^m \tag{1}$$

is used. The values of a and n are taken from Ref. 9, and, expressing G_O in kg/(m^{2}s), the regression rate is computed as

$$r = 7 \times 10^{-6} G_O^{0.8} \text{ m/s} \tag{2}$$

The assumption $n = 0.8$ is also confirmed by some experimental data[17] because the chamber pressure in the present study is usually lower than 6 bar. This is consistent with turbulent diffusion-dominated regression.

The selected grain geometry is a single-port circular section. This simple geometry allows for minimum sliver. Therefore,

$$\frac{\mathrm{d}R}{\mathrm{d}t} = r = a\left(\frac{\mu_O}{A_p}\right)^n \propto \frac{\mu_O^{0.8}}{R^{1.6}} \tag{3}$$

It is also assumed that the regression rate is uniform along the port axis, while no pyrolysis of the lateral ends occurs. Pressure losses inside the combustion chamber are taken into account by relating the chamber head-end pressure p_1 to the chamber nozzle stagnation pressure p_c using an approximate relation similar to that proposed by Barrere et al.[18] for side-burning grains

$$p_1 = (1 + 0.2J^2)p_c \tag{4}$$

which is reliable for $J \leq 0.9$. The hydraulic resistance Z in the oxidizer flow path from the tank to the combustion chamber determines the oxidizer flow rate. Under the assumption of incompressible turbulent flow,

$$\frac{\mathrm{d}m_O}{\mathrm{d}t} = \mu_O = \sqrt{(p_t - p_1)/Z} \tag{5}$$

The value of Z is assumed to be constant unless otherwise specified. The fuel mass flow is

$$\frac{\mathrm{d}m_F}{\mathrm{d}t} = \mu_F = \rho_F r A_b = K_F \mu_O^n = K_F \mu_O^{0.8} \tag{6}$$

where

$$K_F = \frac{a\rho_F A_b}{A_p^n} \propto \frac{1}{R^{0.6}} \tag{7}$$

According to Eqs. (3), (6), and (7), the mixture ratio depends on the oxidizer flow rate and the port radius

$$\alpha = \frac{\mu_O}{\mu_F} = \frac{\mu_O^{(1-n)}}{K_F} \propto \mu_O^{0.2} R^{0.6} \tag{8}$$

Assuming an isentropic expansion in the nozzle, the chamber nozzle stagnation pressure p_c is determined by

$$p_c = \frac{(\mu_O + \mu_F)c^*}{A_t} = \frac{\left(\mu_O + K_F \mu_O^{0.8}\right)c^*}{A_t} \tag{9}$$

Design Parameters and Initial Engine Geometry

According to the assumed ballistic model, the initial design of the HRE is defined when four parameters are given. The four parameters that are chosen here are the initial mixture ratio α_i, the initial thrust level F_i, the initial chamber pressure $(p_c)_i$, and the ratio J of the throat area to the initial port area.

When α_i is known, c^*, C_F, and c can be evaluated via the curve fits presented in Fig. 1. The mass flow rates at the rocket's first ignition (i.e., at $t = 0$) are found for the given value of the initial thrust F_i

$$(\mu_p)_i = (1 + \alpha_i)(\mu_F)_i = (1 + \alpha_i)/\alpha_i(\mu_O)_i = F_i/c \tag{10}$$

The areas A_t and $(A_p)_i$ are

$$A_t = (\mu_p)_i/(p_c)_i c^*, \qquad (A_p)_i = A_t/J \tag{11}$$

As stated earlier, the nozzle throat area A_t is considered to be constant during operation. One also deduces

$$(A_b)_i = \frac{(A_p)_i^n}{\rho_F a}\frac{(\mu_F)_i}{(\mu_O)_i^n} \tag{12}$$

The initial port radius R_i and the fuel grain length L are consequently obtained, and the initial engine geometry is defined.

When a fifth parameter is given, that is, the initial tank pressure $(p_t)_i$, Z can be determined by applying Eq. (5) at $t = 0$. Other parameters, which depend on the oxidizer flow rate control strategy and which will be specified in the following, must then be added to define the engine operation. When the relevant parameters are assigned and the initial mass of the satellite is given, Eqs. (2), (5), (6), and

$$\frac{\mathrm{d}V}{\mathrm{d}t} = \frac{F}{m_i - m_O - m_F} \tag{13}$$

can be integrated to provide the port radius, oxidizer and fuel masses, and velocity increment. The integration is stopped when the required ΔV is attained. The tank volume, the grain external radius, and the case geometry are easily derived.

It is assumed that the initial mass of the satellite (payload mass plus propulsion system mass) is $m_i = 100$ kg, while the required velocity increment is $\Delta V = 160$ m/s. The chosen velocity increment roughly corresponds to a three-year stationkeeping of a geostationary satellite. A "launcher point of view" is adopted, as the initial satellite mass is given. However, the optimization algorithm is also able to solve other problems. For instance, if the payload mass is given, one can integrate the relevant equations backwards, from engine burnout to the initial time. Other approaches could be used, for example, the total impulse could be posed instead of the velocity increment. Similar results are obtained.

Optimal Design

The propulsion system mass m_e is the figure of merit on which attention is focused, but other aspects, such as thrust uniformity and engine dimensions, will also be considered in the following. A simple engine configuration,[9] with a cylindrical case, conical nozzle, and one spherical propellant tank is considered; a spherical gas pressure vessel is added when required. The mass of the propulsion system m_e includes the masses of the propellants, the pressurizing gas (He), the combustion chamber, including the insulating liner, the spherical propellant tank, and the spherical pressurizing auxiliary tank, when required. One should note that the nozzle, mixer, valves, ducts and catalyst-bed masses are not included in m_e. These can be considered to be constant for a given oxidizer flow rate control and do not influence the search for the optimum design. On the other hand, these masses should be taken into account when a comparison of the different systems is performed.

The tank and case are made of titanium with a minimum wall thickness of 0.5 mm because it is difficult to machine to lower thickness and maintain tolerances.[19] The insulator liner, which protects the case wall against the combustion gases, has a thickness of 6 mm, and its density is assumed to be equal to that of the PE.

An efficient parametric optimization code that was developed at the Politecnico di Torino is used to find the set of design parameters that maximizes the payload mass, while satisfying the constraints that are imposed on the operative or geometrical parameters of the system. The design parameters are collected in the vector $\boldsymbol{x}$, and the constraints are posed in the form $\boldsymbol{\chi}(\boldsymbol{x}) = 0$. A vector of adjoint constants $\boldsymbol{k}$ is associated with the constraint equations, and the modified performance index $\varphi = m_u + \boldsymbol{k}^{\mathrm{T}}\boldsymbol{\chi}$ is introduced; φ coincides with m_u when the constraints are fulfilled. An algebraic system is obtained by simultaneously enforcing the constraint equations and nullifying the numerically computed partial derivatives of φ with respect to the design parameters. Tentative values are assumed for the design parameters and adjoint constants and are progressively corrected to satisfy the equations by means of a procedure based on Newton's method.

Blowdown Feed System

A simple blowdown system is first considered. No oxidizer flow rate control is present in this case. The pressurizing gas and the propellant are stored in the same tank. In the following, it is assumed that the pressurizing gas is helium and that the expansion is isothermal ($m = 1$). This assumption is used to consider the best performance that can be ideally obtained using blowdown. If one or a few extensive maneuvers are performed, an isentropic expansion should in fact be considered, whereas, if multipulses are used, ignition transients should be taken into account. The authors found however that the influence of the nature of the gas and the kind of expansion is weak. The tank pressure can be evaluated as

$$p_t = (p_t)_i (V_g)_i / V_g \tag{14}$$

A sixth parameter, the initial pressurizing gas volume $(V_g)_i$, is then required to define engine operation.

Parametric Study

The design choices influence the value of the regression rate during operations. The minimum regression rate $r_{\min}$ should not be lower than a critical value r_{cr} to avoid "cooking" of the subsurface layers in the solid grain, leading to poor combustion caused by fuel charring, softening or melting. A parametric study was performed to highlight how the choice of J and α_i affects the engine design. The results are shown in Fig. 2. A different engine is designed for any

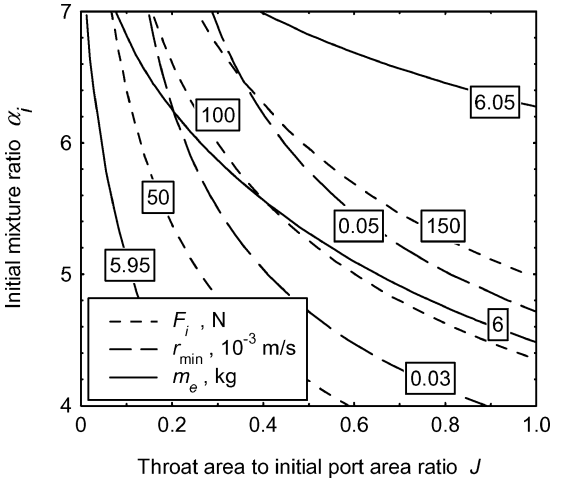

Fig. 2 Initial thrust level, propulsion system mass, and minimum regression rate as a function of the initial mixture ratio and throat to the initial port area ratio.

given couple of values $[J, \alpha_i]$. Figure 2 shows contour lines of the propulsion system mass m_e, of the minimum regression rate during operation $r_{\min}$, and of the initial thrust level F_i.

It appears that m_e can be reduced by lowering F_i. However, this choice also reduces the regression rate (whereas the burning time is obviously increased), and the aforementioned subsurface cooking could occur. The constraint $r_{\min} = r_f = r_{\text{cr}}$ is therefore posed. A value $r_{\text{cr}} = 0.03$ mm/s is chosen.[9]

When the value of J is also assigned, the influence of α_i can be analyzed separately. The dashed lines in Fig. 3 present m_e as a function of the initial mixture ratio α_i for a given value of J. It clearly appears that an optimum value of α_i exists for each value of J. The continuous line joins the minimum-m_e points of each curve. The full circle indicates the optimal J, α_i combination.

Optimal Design

The optimization procedure is used here to provide the values of α_i, F_i, and J that minimize the value of m_e, while fulfilling the constraint on the minimum regression rate. The values of $(p_t)_i$, $(p_c)_i$, and $(V_g)_i$ are assigned and kept constant because they only influence the optimal value of m_e weakly. Therefore, the values $(p_t)_i = 10$ bar, $(p_c)_i = 6$ bar, and $(V_g)_i = 4 \times 10^{-3}$ m^3 are assumed, unless otherwise specified.

Going back to Fig. 2, one can realize that there exists a constant-m_e curve that is tangent to the constant-$r_{\min}$ curve for the assumed value $r_{\min} = r_{\text{cr}}$. The contact point of these two curves corresponds to the optimal solution. One should be aware that a thermal chocking could arise (i.e., the optimal J can increase above unity). Therefore, the constraint $J \leq 0.9$ is imposed in the following when required. If we look again at Fig. 2, it appears that this situation occurs if larger values of $r_{\min} = r_{\text{cr}}$ are assumed.

Figure 4 shows that p_t, p_c, μ_O, μ_F, and F decrease during operations, while the mixture ratio α increases. The thrust reduction is quite remarkable as the ratio of the initial thrust to the final thrust is 1.63 (see Table 1 for further details). The specific impulse is not constant during operations but shifts according to the changes of the propellant mixture ratio. The optimal solution makes the mean mixture ratio close to the value that maximizes the specific impulse, to reduce the propellant mass.

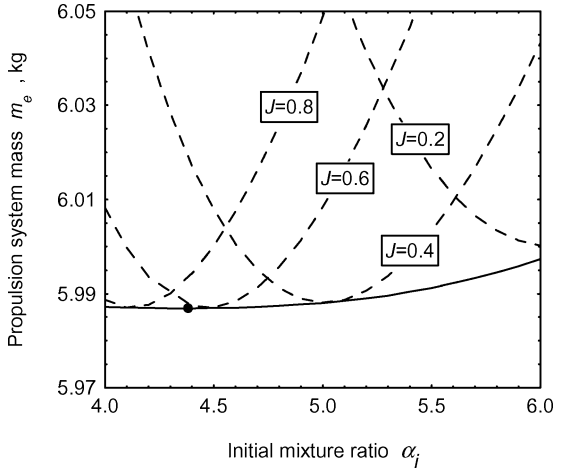

Fig. 3 Propulsion system mass as a function of the initial mixture ratio and throat to the initial port area ratio.

As an example, Figs. 5 and 6 show the effect of the initial value of the volume of the pressurizing gas on the optimal design. The aforementioned constraint $J \leq 0.9$ is active for $(V_g)_i < 2700$ cm^3. The trend of the curves in Figs. 5 and 6 does not seem to be affected by this constraint. The overall length L, that is, the sum of the length of the propellant tank, case, and nozzle, undergoes a slight variation, presenting a minimum for $(V_g)_i$ 3130 cm^3. The propellant tank diameter, which is the largest width, is increased with $(V_g)_i$

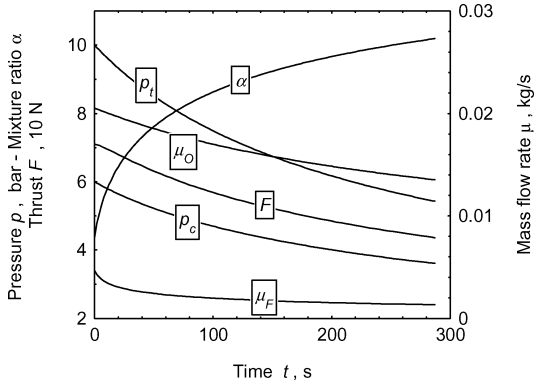

Fig. 4 Blowdown ($J = 0.643$, $m_e = 5.99$ kg).

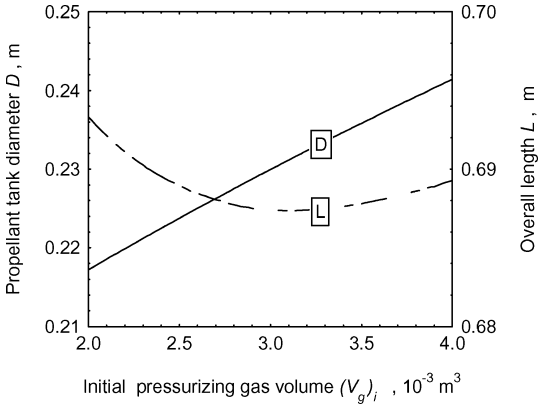

Fig. 5 Influence of the initial gas volume on the propulsion system dimensions.

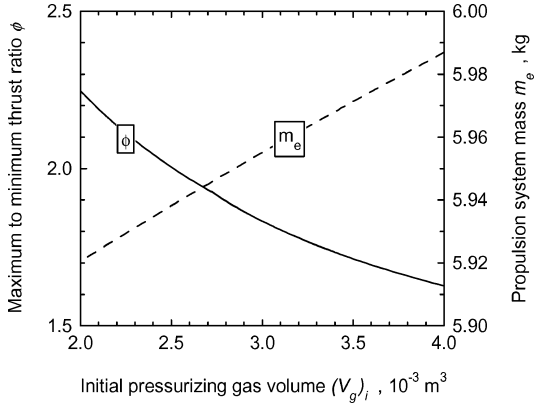

Fig. 6 Influence of the initial gas volume on the propulsion system mass and thrust variation.

Table 1 Performance comparison

Oxidizer control	Auxiliary tank	$(\alpha)_i$	J	$(F)_i$, N	ΔF, N	Length, m	Width, m	m_e, kg
Blowdown	N	4.383	0.643	71.0	27.4	0.69	0.24	5.99
Constant α ($\alpha = 8.745$)	N	8.745	0.900	466.9	422.0	0.96	0.24	6.02
Repressurization ($p_r = 7.3$ bar)	Y	4.427	0.436	56.5	12.3	0.73	0.24	6.01
Constant p_c ($p_c = 6$ bar)	Y	4.361	0.306	43.9	1.0	0.68	0.19	5.91
Constant p_t ($p_t = 10$ bar)	Y	4.357	0.335	46.3	1.6	0.70	0.19	5.92

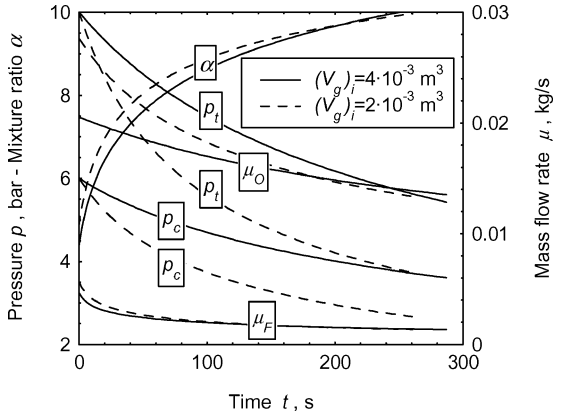

Fig. 7 Influence of the initial gas volume on the tank and chamber pressure levels, mass flows, and mixture ratio during operation.

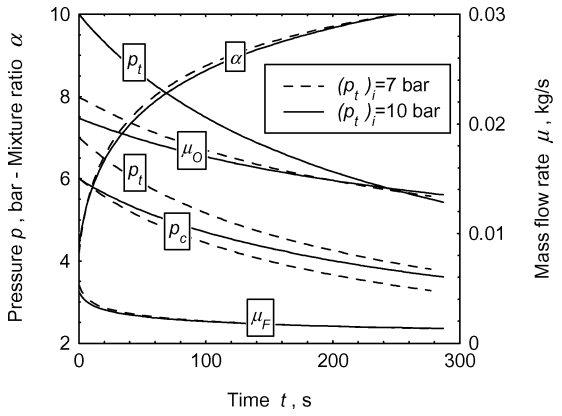

Fig. 8 Influence of the initial gas pressure on the tank and chamber pressure levels, mass flows, and mixture ratio during operation.

because the oxidizer mass and volume do not vary to any great extent. The propulsion system mass m_e increases slightly, while the thrust ratio decreases. A larger initial volume of gas could therefore be convenient when enough space is available because it reduces the variation of gas pressure and performance during operations. This is also highlighted in Fig. 7, where the oxidizer and fuel mass flows are represented as a function of time, together with the tank and chamber pressures for two values of $(V_g)_i$. Figures 5–7 suggest that the choice of $(V_g)_i$ should be mainly directed by considerations concerning operation uniformity and available space in the spacecraft.

The initial pressure levels also seem to affect the value of m_e weakly. Higher pressure in the tank and combustion chamber reduces the variation of the mixture ratio during operations. The benefit, in terms of propellant mass, is balanced by the larger gas mass and wall thickness. The mass of the propulsion system does not change remarkably, with a slight increment of m_e when the tank pressure is increased. Some characteristic quantities during operations are shown in Fig. 8 for two different values of the tank pressure. The effect of a larger tank pressure is similar to that of larger volumes of pressurizing gas and produces a more uniform combustion process.

Oxidizer Flow Rate Control

Because of the oxidizer flow rate control capability, HREs are similar to liquid rocket engines (LREs). The solutions that are adopted to control liquid propellants in LREs can give an insight into the benefit of controlling the oxidizer with respect to a simple blowdown feed system. Bipropellant LREs generally require a regulated pressure system to keep the mixture ratio at the given optimum value. On the other hand, as far as monopropellant hydrazine thrusters with blowdown are concerned, the specific impulse decreases with pressure decay, because of the greater ammonia dissociation. A regulated pressure system could solve this problem, while also ensuring a constant thrust during operations. However, the penalty of greater complexity and heavier weight must be considered. An intermediate solution, used for instance in the Magellan[20] propulsion system, is repressurization in conjunction with blowdown. One or more recharges are used to raise the propellant tank pressure when a prescribed minimum value is reached during blowdown operations. Recharge gas requires an auxiliary tank, which is normally connected to the propellant tank via an ordnance valve.

Several oxidizer flow rate control strategies are considered in this paper for an HRE.

Constant Mixture Ratio

In the blowdown system, a mixture-ratio shifting occurs. This problem, which does not affect LREs, can be avoided if the oxidizer is controlled to keep the mixture ratio constant. The so-called dual-mode oxidizer injection scheme, wherein a second injection is used to trim the mixture ratio in an aft combustion chamber, is not considered here because this system requires a more complex control system. Two mass flows should in fact be controlled in this scheme.

The expected benefit, that is, the reduction of the propellant mass, is maximum when the mixture ratio is kept at the value that corresponds to the maximum effective exhaust velocity. If c is constant, the required propellant mass can be easily evaluated:

$$m_p = m_i \frac{e^{\Delta V/c} - 1}{e^{\Delta V/c}} \tag{15}$$

As $c_{\max} = 3013$ m/s (for $\alpha = 7.55$), the propellant mass is $m_p = 5.17$ kg while it is 5.23 kg in the blowdown case. The expected benefit is therefore 0.06 kg. The propellant mass reduction is however overcome by a larger structural mass. Moreover, a very large thrust variation occurs unless the dual-mode oxidizer injection scheme is adopted; according to Eq. (8), if α is kept constant

$$\mu_O \propto R^3 \tag{16}$$

and a strong variation of μ_O is required. According to Eq. (20), this can be obtained either by varying Z or with a large variation of p_t. The required tank pressure p_t is shown in Fig. 9 for $\alpha = 7.55$, when Z is kept constant, and is compared with isothermal and adiabatic expansion of the pressurizing gas. Because the required p_t is lower than the adiabatic expansion, a depressurization is necessary; no auxiliary gas is required, and the control system is defined via $(V_g)_i$, as in the blowdown system case.

The helium vented from the propellant tank could be introduced into the combustion chamber (into the head or into the mixer aft the grain), and it would only affect the performance slightly, as the addition of helium modifies gas combustion properties. As an example, Fig. 10 shows the effect of the helium addition on the

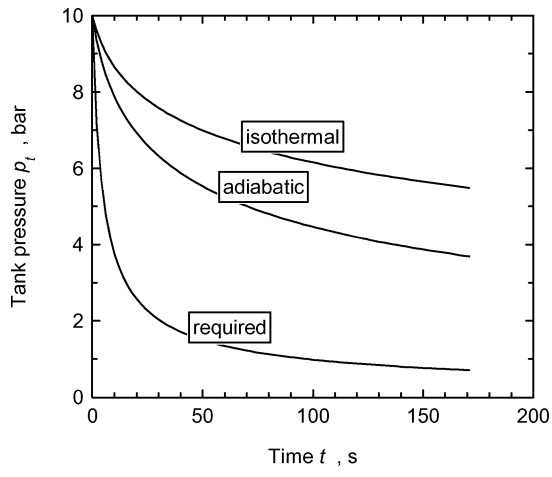

Fig. 9 Tank pressure for a constant mixture-ratio control ($\alpha = 7.55$).

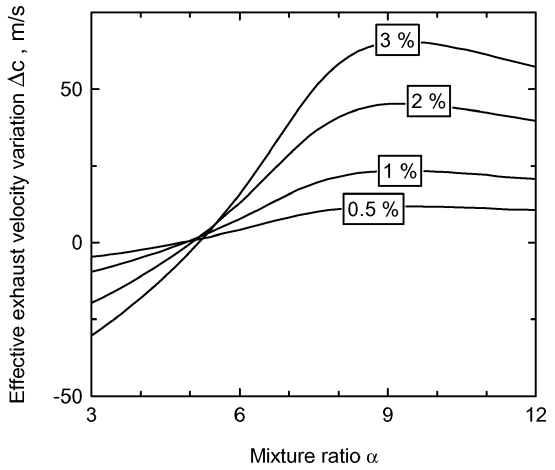

Fig. 10 Effect of helium on the effective exhaust velocity. (The percentage is the helium mass to helium plus HP mass.)

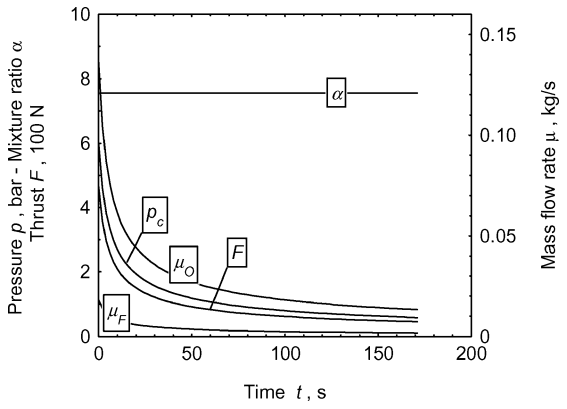

Fig. 11 Constant mixture-ratio control: $\alpha = 7.55$ ($J = 0.900$, $m_e = 6.02$ kg).

effective exhaust velocity c. Note that the helium is considered as a part of the oxidizer flow. It appears that the addition of helium determines a performance benefit when the mixture ratio is in the range of interest. Moreover, the temperature of the exhaust gas is lowered, thus reducing heat loads. On the other hand, the helium mass is small compared to the propellant mass, and the effect on the whole engine performance is also small. The effect of helium flow is therefore neglected in the following.

Figure 11 shows the behavior of the engine during operations when $\alpha = 7.55$, which corresponds to the maximum specific impulse. The constraint $J \leq 0.9$ is active, as usually occurs with this control strategy, and only a single parameter (namely, the initial thrust level) can be optimized. A very large variation of the thruster operation parameters occurs. As an example, the maximum to minimum thrust ratio is 10.3. The propulsion system mass is $m_e = 6.02$ kg against the 5.99 kg of the blowdown case.

Figure 12 shows the propellant and structural mass variation as a function of α. Because of the different propellant densities, volumetric loading fraction, and tank/case shape, it is preferable to use more oxidizer than that required to obtain the maximum specific impulse: the minimum engine mass is obtained for $\alpha = 8.745$. In this case the trends of the operating parameters are similar to those presented in Fig. 11 and are therefore not shown.

The engine results to have a longer length (see Table 1). This is mainly caused by a longer nozzle because the high initial thrust level determines a large throat area. This fact causes an additional penalty in terms of engine mass, which is not considered here.

Repressurization

A single-shot repressurization is considered in conjunction with a blowdown system. The auxiliary gas is stored at a pressure p_a in a separate tank and released when the propellant tank pressure reaches the given value p_r. The auxiliary gas mass raises the propellant tank pressure to the initial value $(p_t)_i$. With respect to the blowdown system, two additional design parameters, namely, p_a and p_r, are introduced.

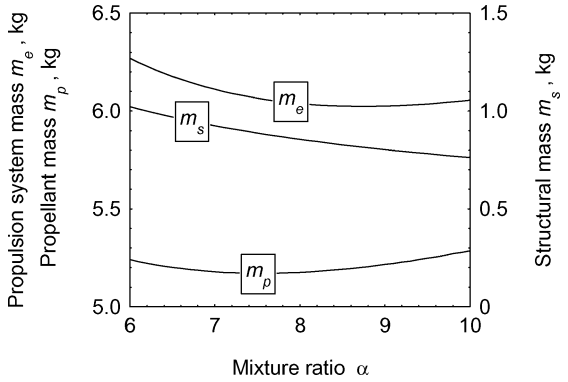

Fig. 12 Constant mixture-ratio control: effect on the propellant, structural and propulsion system mass.

The following simplifying assumptions are made to evaluate the auxiliary gas mass: the repressurization process is adiabatic, the pressure in the gas tank and in the propellant tank is the same at the end of the repressurization, and the gas pressure rise caused by the heat exchange after repressurrizing is neglected. By indicating the llage volume when $p_t = p_r$ with $(V_g)_r$, and the auxiliary gas tank volume with V_a,

$$\frac{V_a}{(V_g)_r} = \frac{(p_t)_i - p_r}{p_a - (p_g)_i} \tag{17}$$

Thus, the mass of axiliary gas and relative tank is easily computed.

Repressurization determines an oxidizer mass flow increment that slightly increases the regression rate and the mixture ratio. To understand these effects, one can consider the oxidizer mass flow μ_O as the control variable for a given grain geometry (i.e., the geometry at a prescribed instant of engine operations). According to Eq. (8), for a given value of R, one obtains

$$\alpha \propto \mu_O^{0.2} \tag{18}$$

whereas, according to Eq. (3), the regression rate is

$$r \propto \mu_O^{0.8} \tag{19}$$

On the other hand, the relation between the tank pressure and the oxidizer mass flow is

$$Z\mu_O^2 + \left(c^*/A_t\right)\left(\mu_O + K_F\mu_O^{0.8}\right) = p_t \tag{20}$$

The repressurization pressure cannot be lower than a certain level to satisfy the minimum regression-rate constraint. For the prescribed values, p_r must be higher than 6.3 bar. Therefore, $6.3 \leq p_r \leq 10$ bar. In this pressure range, Eq. (20), at a given time, is well fitted with a straight line

$$p_t = 7 \times 10^7 \mu_O - \delta \tag{21}$$

where δ only depends on the thruster geometry and, therefore, on the operation time. As an example, when $p_r = 8$ bar, $\delta = 2.5\ 10^5$ Pa at $t = 0$ and $\delta = 2.74\ 10^5$ Pa at the repressurization time. It thus appears that repressurization is able to recover the initial oxidizer mass flow when the initial tank pressure is restored. As far as the recovering of the chamber pressure is concerned, the fuel flow is lower because of the larger port area, but repressurization occurs when α is large and the contribution of fuel flow to the total flow is weak; therefore, the chamber pressure and thrust level are also recovered. The advantage of repressurization is that the thrust variation is reduced. This reduction is obtained in spite of the small increment of the engine mass and volume (the auxiliary gas tank), whereas the

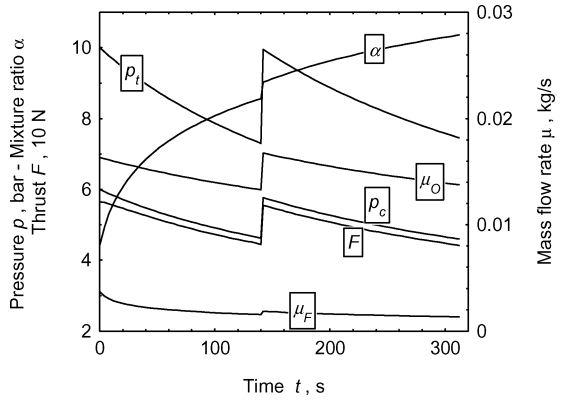

Fig. 13 Blowdown with single-short repressurization: $p_r = 7.3$ bar ($J = 0.436$, $m_e = 6.01$ kg).

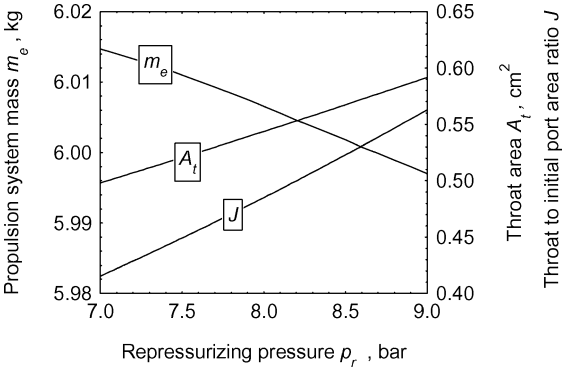

Fig. 14 Parameter variation as a function of the repressurizing pressure.

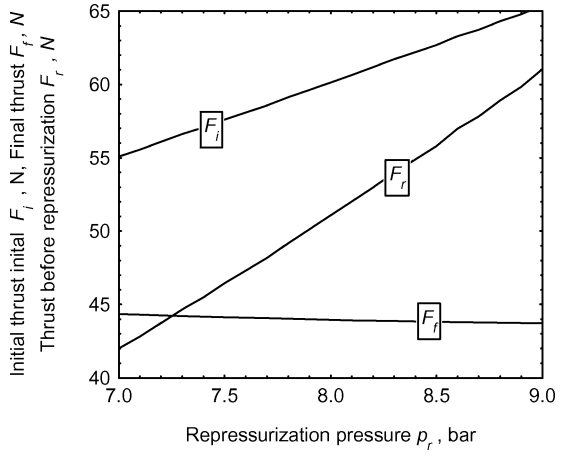

Fig. 15 Initial thrust, final thrust, and thrust before repressurization as a function of the repressurizing pressure.

mixture ratio shifting is almost the same as in the blowdown case. As an example, Fig. 13 shows the engine operation for $p_r = 7.3$ bar, which corresponds to a case where the thrust before repressurization and at the final time have similar values.

As far as the two new parameters are concerned, p_a has a negligible effect on the engine mass, engine geometry and operations, and is set to a fixed value, namely, $p_a = 150$ bar. On the other hand, p_r does not appreciably affect the engine mass, while it modifies the engine design and operations. The propulsion system mass presents a very small increment as p_r decreases, as shown in Fig. 14. The variations of the throat area A_t and of the area ratio J are instead remarkable. Figure 15 shows the thrust level at the initial and final times and just before repressurization. The thrust levels

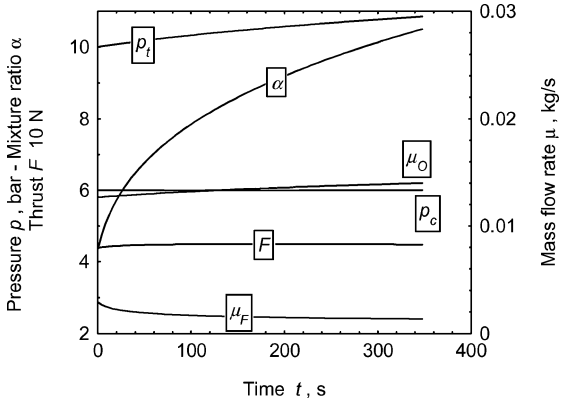

Fig. 16 Constant chamber pressure control: $p_c = 6$ bar ($J = 0.306$, $m_e = 5.91$ kg).

at the end of operations and before repressurization are equal when $p_r \sim 7.3$ bar.

Constant Chamber Pressure

An oxidizer flow rate control that keeps the chamber pressure constant during operation is able to guarantee a quasi-constant thrust because

$$F = p_c A_t C_F \tag{22}$$

and the throat area erosion and mixture shifting effects on the thrust coefficient can be neglected.

Equation (9) can be used to compute the required oxidizer mass flow, while Eqs. (5) and (4) are used to determine the corresponding p_t. An auxiliary pressurizing tank is therefore required to keep the tank pressure at the prescribed value. The work W performed by the gas on the liquid propellant can be evaluated as

$$W = \int p_t \, \mathrm{d}V = \int p_t \frac{\mu_O}{\rho_O} \, \mathrm{d}t \tag{23}$$

The initial pressurizing gas volume $(V_g)_i$ is no longer a design parameter, while the auxiliary tank volume and pressurizing gas mass have to be computed. To have a stable regulator response,[21] it is assumed that the initial ullage volume V_u is 3% of the propellant tank. A valve pressure loss $\Delta p_v = 3$ bar is also assumed. The volume of the tank that contains the pressurizing gas can be easily computed

$$V_a = \frac{(\gamma - 1)W + (p_t)_f (V_t)_i - (p_t)_i V_u}{p_a - [(p_t)_f + \Delta p_v]} \tag{24}$$

Figure 16 shows the trend of the relevant parameters during operations. The thrust level undergoes a very small increment during operations. (The maximum to minimum thrust ratio is 1.02.) The engine results in being more compact (the pressurizing gas is stored at higher pressure) and lighter than in the blowdown reference case, as shown in Table 1.

Constant Tank Pressure

A similar result can be obtained via an oxidizer flow rate control, which is similar to that used with LREs, which results in being simpler, that is, by imposing a constant tank pressure p_t. The same assumptions about the ullage volume and valve pressure drop are made as in the preceding subsection. The work performed by the gas on the liquid oxidizer is $W = p_t V_O$, and Eq. (24) becomes

$$V_a = \frac{\gamma p_t V_O}{p_a - [p_t + \Delta p_v]} \tag{25}$$

Figure 17 shows the engine operations in this case. The dimensions and weight are comparable with the constant chamber pressure control. The chamber pressure and thrust level are almost constant.

Table 2 Effects of nozzle area ratio on the engine design in the blowdown case

ε	$(\alpha)_i$	J	$(F)_i$, N	ΔF, N	Length, m	Width, m	m_e, kg
80	4.27	0.703	71.1	27.7	0.68	0.24	6.03
100	4.38	0.643	71.0	27.4	0.69	0.24	5.99
120	4.44	0.615	70.9	27.1	0.71	0.24	5.94

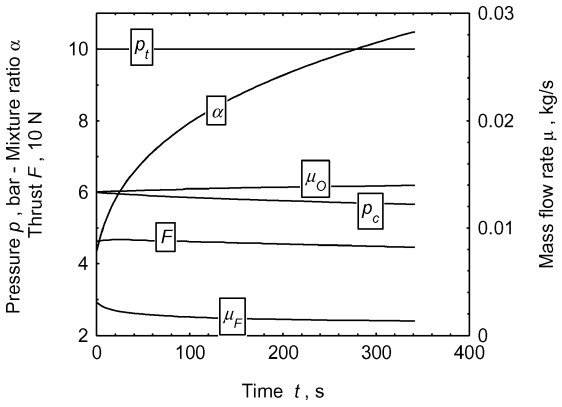

Fig. 17 Constant tank pressure control: $p_t = 10$ bar ($J = 0.335$, $m_e = 5.92$ kg).

Nozzle Mass and Nozzle Area Ratio Effects

The nozzle mass was not included in the preceding analysis. Many factors, such as nozzle erosion rate, burn time, nozzle throat area, and nozzle area ratio, influence the nozzle mass. On the other hand, these factors are not independent. According to literature,[22] the nozzle mass of solid rocket motors is approximately proportional to the total impulse. The nozzle mass has no effect on the optimal solution if this assumption is retained.

A more detailed estimation of the nozzle mass should be used to analyze the effect of the nozzle area ratio value. An increase of ε results in both an increase of the effective exhaust velocity and the nozzle mass so that is necessary to reach a compromise between these two factors. Moreover, because the geometrical envelope is also a critical design constraint, the nozzle length must be limited. The nozzle mass variation, with respect to the $\varepsilon = 100$ case, has been evaluated using the following relation:

$$\Delta m_n = \frac{\beta A_t}{\sin(15\,\text{deg})}(\varepsilon - 100) \tag{26}$$

The value of β is fixed throughout as twice the product of the titanium density times the combustion chamber wall thickness. A surface fit of the thrust coefficient, computed via a popular code[16] as a function of α and ε, is introduced into the code to compute the proper values, for the given nozzle area ratio, as the mixture ratio changes during engine operations. Table 2 shows some results for the blowdown case; small variations of the optimal design parameters and engine mass are obtained. The engine mass m_e does not include the whole nozzle mass but only its variation as evaluated in Eq. (26), in order to allow a direct comparison with the results of Table 1. A larger nozzle area ratio would determine a limited benefit in terms of engine mass, whereas the engine length would be augmented.

Conclusions

The present work focuses on the parameters that affect the design of an HRE for small satellites and the benefit that can be obtained when using an oxidizer flow rate control.

The relevant parameters are identified. Four parameters, namely, the initial mixture ratio, the initial thrust level, the initial chamber pressure, and the ratio of the throat area to the initial port area, determine the initial geometry. A fifth parameter, the initial propellant tank pressure, determines the hydraulic resistance of the feed system. Other parameters might be required that depend on the chosen oxidizer flow rate control. The optimal design is found by means of a parametric optimization, and the effect of the design parameters on the propulsion system mass is highlighted and discussed. A constraint on the minimum regression rate must be imposed to avoid solutions that experience grain cooking. A constraint on the throat to initial port area ratio might also be necessary. In the blowdown case, just three parameters (here the initial mixture ratio α_i, the initial thrust level F_i, and the initial port area to throat area ratio J) identify the optimal design.

As far as the oxidizer flow rate control is concerned, four different control strategies are considered and compared to the blowdown case. Table 1 shows the main features of the HRE for the different oxidizer flow rate controls here considered. The overall system mass exhibits small variations even though some cases require an auxiliary tank because its mass is almost integrally balanced by the reduction of the case and propellant masses. The length represents the sum of the nozzle, chamber, and tanks, while the width is the largest dimension (namely the spherical propellant tank). The nozzle length is computed considering a conical nozzle with a 60-deg half-angle for the convergent cone section and a 15-deg half-angle for the divergent cone. The constant mixture ratio control appears to be the worst case, when the propulsion system mass, dimensions, and behavior uniformity during operation are considered. The repressurization presents the benefit of thrust uniformity. The constant pressure control (both chamber pressure and propellant tank pressure) presents a good thrust uniformity, and the engine is more compact. The overall mass benefit that is presented here is actually overcome by the more complicated system that is necessary compared to the blowdown case. The simplest blowdown feed system is preferable unless a space or thrust level constraint is posed.

Acknowledgment

The authors gratefully acknowledge Agenzia Spaziale Italiana for its support in this research.

References

[1]Sackheim, R., Ryan, R., and Threet, E., "Survey of Advanced Booster Option for Potential Shuttle-Derivative Vehicles," AIAA Paper 2001-3414, July 2001.

[2]Schoonover, P. L., Crossley, W. A., and Heister, S. D., "Application of a Genetic Algorithm to the Optimization of Hybrid Rockets," *Journal of Spacecraft and Rockets*, Vol. 37, No. 5, 2000, pp. 622–629.

[3]Ventura, M. C., and Heister, S. D., "Hydrogen Peroxide as an Alternate Oxidizer for a Hybrid Rocket Booster," *Journal of Propulsion and Power*, Vol. 11, No. 3, 1995, pp. 562–565.

[4]Vonderwell, D. J., Murray, I. F., and Heister, S. D., "Optimization of Hybrid-Rocket-Booster Fuel-Grain Design," *Journal of Spacecraft and Rockets*, Vol. 32, No. 6, 1995, pp. 964–969.

[5]Werthman, W. L., and Schroeder, C. A., "A Preliminary Design Code for Hybrid Rockets," AIAA Paper 94-0006, Jan. 1994.

[6]Ben-Yakar, A., and Gany, A., "Hybrid Engine Design and Analysis," AIAA Paper 93-2548, June 1993.

[7]Jansen, D. P. F. L., and Kletzkine, Ph., "Preliminary Design for a 3kN Hybrid Propellant Engine," *ESA Journal*, Vol. 12, No. 4, 1988, pp. 421–439.

[8]Yuasa, S., Yamamoto, K., Hachiya, H., Kitagawa, K., and Owada, Y., "Development of a Small Sounding Hybrid Rocket with a Swirling-Oxidizer-Type Engine," AIAA Paper 2001-3537, July 2001.

[9]Maisonneuve, Y., Godon, J. C., Lecourt, R., Lengelle, G., and Pillet, N., "Hybrid Propulsion for Small Satellites: Design Logic and Test," *Combustion of Energetic Materials*, edited by K. K. Kuo and L. T. De Luca, Begell House, New York, 2002, pp. 90–100.

[10]Sellers, J. J., Meerman, M., Paul, M., and Sweeting, M., "A Low-Cost Propulsion Option for Small Satellites," *Journal of the British Interplanetary Society*, Vol. 48, No. 3, 1995, pp. 129–138.

[11]Morring, F., Jr., "Test Puts Hybrid Rockets Back on the Table," *Aviation Week and Space Technology*, Vol. 158, No. 5, 2003, pp. 50, 51.

[12]Dornheim, M. A., "Affordable Spaceship," *Aviation Week and Space Technology*, Vol. 158, No. 16, 2003, pp. 64–73.

[13]Karabeyoglu, M. A., Altman, D., and Cantwell, B. J., "Combustion of Liquefying Hybrid Propellants: Part 1, General Theory," *Journal of Propulsion and Power*, Vol. 18, No. 3, 2002, pp. 610–620.

[14]Karabeyoglu, M. A., and Cantwell, B. J., "Combustion of Liquefying Hybrid Propellants: Part 1, General Theory," *Journal of Propulsion and Power*, Vol. 18, No. 3, 2002, pp. 621–630.

[15]Colasurdo, G., Pastrone, D., and Casalino, L., "Optimal Propellant Control in Hybrid Rocket Engines," AIAA Paper 95-2393, July 1995.

[16]McBride, B. J., and Reno, M. A., "CET93 and CETPC: An Interim Updated Version of the NASA Lewis Computer Program for Calculating Complex Chemical Equilibria With Applications," NASA TM-4557, March 1994.

[17]Wernimont, E. H., and Heister, S. D., "Combustion Experiments in Hydrogen Peroxide/Polyethylene Hybrid with Catalitic Ignition," *Journal of Propulsion and Power*, Vol. 16, No. 2, 2000, pp. 218–326.

[18]Barrere, M., Jaumotte, A., De Veubeke, B. F., and Vandenkerckhove, J., *Rocket Propulsion*, Elsevier, Amsterdam, 1960, Chap. 5, pp. 251–256.

[19]Brown, C. D., *Spacecraft Propulsion*, Monopropellant Systems, AIAA Education Series, AIAA, 1996, Chap. 4, p. 84.

[20]Brown, C. D., *Spacecraft Propulsion*, Monopropellant Systems, AIAA Education Series, AIAA, 1996, Chap. 4, pp. 104–106.

[21]Brown, C. D., *Spacecraft Propulsion*, AIAA Education Series, AIAA, 1996, p. 82.

[22]Barrere, M., Jaumotte, A., De Veubeke, B. F., and Vandenkerckhove, J., *Rocket Propulsion*, Design of Solid-Propellant Rockets, Elsevier, Amsterdam, 1960, Chap. 6, p. 317.